Journal of Solid State Chemistry **149,** 218–225 (2000)
doi:10.1006/jssc.1999.8507, available online at http://www.idealibrary.com on IDEAL®

An Electron Diffraction and XRD Study of the α_1' and α_1'' Fluorite-Related Phases in the $(1-x)\frac{1}{2}Bi_2O_3 \cdot xCaO$, $0.20 < x < 0.29$, System

R. L. Withers,[1] A.-K. Larsson,* and S. Schmid

*Research School of Chemistry, Australian National University, Canberra, ACT, 0200 Australia; and *Inorganic Chemistry, Arrhenius Laboratory, Stockholm University, S-106 91 Stockholm, Sweden*

Two fluorite-related modulated phases (α_1' and α_1'') occurring in the $(1-x)\frac{1}{2}Bi_2O_3 \cdot xCaO$, $0.20 < x < 0.29$, system have been carefully investigated via electron diffraction and XRD. The satellite reflections accompanying the strong fluorite-type substructure Bragg reflections were always found to be of $G_F \pm \sim \frac{1}{8}\langle 224\rangle_F^*$ (F for fluorite)-type and to be consistent with a lowering of the cubic $m3m$ point group symmetry of fluorite to rhombohedral $\bar{3}m$ point group symmetry in both cases. The type of rhombohedral symmetry, however, was found to be quite distinct. The α_1' phase is shown to be a two-dimensional incommensurately modulated phase of $R\bar{3}m(\varepsilon 00)$ 11 superspace symmetry while the α_1'' phase is shown to be a rhombohedral, commensurately modulated, superstructure phase. Ca/Bi metal ion ordering on the essentially ccp cation array is shown to be largely responsible for the observed satellite reflections and an expression for this ordering is derived using a modulation wave approach to structural characterization.

1. INTRODUCTION

The high-temperature fluorite-related polymorph of Bi_2O_3, δ-Bi_2O_3, is one of the best oxygen ion conductors known (1, 2). It cannot, however, be quenched to room temperature. Indeed, a room temperature, fluorite-related phase cannot be obtained without the addition of a certain amount of a dopant metal oxide such as an alkaline earth oxide, a rare-earth oxide or a range of transition metal oxides (3–9). Much work has been devoted over a considerable period of time to the remarkable structural flexibility and oxygen ion transport properties of many such ternary bismuth oxide phases (3–11). In the form of higher temperature solid solution phases, such phases are frequently highly conductive but often undergo phase transitions into related lower temperature phases upon cooling at which desirable transport properties can change significantly (5, 10).

[1]To whom correspondence should be addressed.

One such ternary bismuth oxide phase is the so-called α-type solid solution phase in the $(1-x)\frac{1}{2}Bi_2O_3 \cdot xMO$, $M = Ca$, system (4, 5, 12, 13). The equilibrium phase diagram for this system was first published by Conflant *et al.* (5) and subsequently modified somewhat by Roth and colleagues (12, 13). A face centered cubic (fcc), α-type solid solution phase was reported to exist at elevated temperatures all the way up to a maximum CaO content of $\sim$29 mol%. Conflant *et al.* (5), however, also reported the existence of a small region in the CaO-rich, low-temperature portion of this fcc phase field which differed from a purely cubic disordered fcc structure. In particular, weak (slightly composition-dependent) superstructure reflections were reported as accompanying the strong Bragg reflections of an underlying fcc average structure for x greater than 25 mol% CaO. It is worthwhile to note that these additional satellite reflections were detected at elevated temperature. Given that the solid solution is a good oxygen ion conductor at these elevated temperatures, it is clear that the satellite reflections must primarily arise from Ca/Bi ordering within an essentially ccp cation array. This equilibrium fluorite-related solid solution phase was labelled α_1'.

Conflant *et al.* (5) also reported the existence of a further metastable α_1'' fluorite-related line phase of composition 27.4 mol% CaO obtained by slow cooling the α_1' phase of this composition through a eutectic at 780°C. This phase was also characterized by the existence of satellite reflections (closely related to those of the α_1' phase). Unlike the α_1' phase, however, the strong parent substructure lines of this metastable α_1'' fluorite-related line phase were clearly rhombohedrally split.

Subsequent work by Roth and colleagues (12, 13) has confirmed the existence of both the α_1' and α_1'' phases although somewhat wider composition and temperature ranges of existence for the former phase were found. The additional satellite reflections characteristic of the α_1' phase, for example, were reported as being present in any quenched fcc phase sample containing 20 mol% or more CaO.

0022-4596/00 $35.00

In addition, a slight rhombohedral splitting of the parent substructure reflections was also found (12, 13). This rhombohedral splitting of the parent substructure reflections was found to be greatly enhanced in the α_1'' phase, in agreement with the reported results of Conflant *et al.* (5).

The additional satellite reflections were not indexed in the case of the α_1' phase. The strong substructure reflections were indexed to a rhombohedral $R\bar{3}$ ($a = 7.7427$, $c = 9.465$ Å) unit cell for a 27.27 mol% CaO specimen quenched from 780°C. In the case of the α_1'' phase, it was reported (13) that single crystal X-ray precision patterns and XRD data could be fitted to either a monoclinic ($B2/m$, $a = 15.5819(3)$, $b = 3.8077(1)$, $c = 10.8955(3)$ Å, $\beta = 91.829(2)^\circ$) or rhombohedral ($R\bar{3}$, $a = 30.4640(5)$, $c = 9.6477$ Å) superstructure of an underlying rhombohedrally distorted fluorite-type parent structure.

The purpose of this paper is to investigate via electron diffraction the nature of these two fluorite-related modulated structures.

2. EXPERIMENTAL

Synthesis

Samples were prepared in one of two ways. In the first method, Bi_2O_3 (Atomergic Chemetals Co., 99.999%) and CaO were ground together in the appropriate ratios. (The CaO had previously been prepared by heating $CaCO_3$ (Halewood Chemicals Ltd., 99.999%) for 16 h at 850°C). The ground samples were then pelleted and calcined at 840°C for 2 h on an alumina tile. The specimens were then quenched in liquid N_2, reground, repelleted, and calcined at 840°C for a further 3 h followed by a second quenching, regrinding, repelleting, and a final calcining for 16 h at 840°C. The resultant specimens were then heat treated appropriately.

In the second method, samples were prepared by grinding Bi_2O_3 (Atomergic Chemetals Co., 99.999%) and $CaCO_3$ (Halewood Chemicals Ltd., 99.999%) in the appropriate ratios. These ground samples were then calcined at various temperatures above 800°C for 2–4 h in open gold tubes and then melted for 5 min at 1000°C prior to quenching in water. The samples were then reground and heat treated appropriately. Samples prepared via either approach gave the same experimental results.

Characterization

Specimens were examined by XRD using a Guiner–Hägg camera with monochromated Cu$K\alpha_1$ radiation. For the determination of unit cell dimensions, an internal standard of Si (NBS No. 640) was added to calibrate the measurement of XRD films. Specimens for electron microscopy were prepared by crushing and dispersing onto holey-carbon coated copper grids. These grids were then examined in JEOL 100CX and Philips EM430 transmission electron microscopes (TEMs).

3. RESULTS

Electron diffraction patterns (EDPs) of both phases were dominated by the strong Bragg reflections, $\mathbf{G}_F$ (F for fluorite), of the underlying ($Fm3m$) fluorite-type parent structure (see, for example, the $\langle 111\rangle_F$ and $\langle 110\rangle_F$ zone axis EDP's of Figs. 1 and 2). Accompanying these parent Bragg reflections are a plethora of additional satellite reflections. The strongest satellite reflections characteristic of both the α_1' and α_1'' phases were always found to be of $\mathbf{G}_F \pm \sim\frac{1}{8}\langle 224\rangle_F^*$ type, where $\mathbf{G}_F$ represents the strong Bragg reflections of the underlying ($Fm3m$) fluorite-type parent structure (see, for example, the $\langle 111\rangle_F$ and $\langle 110\rangle_F$ zone axis electron diffraction patterns (EDPs) of Figs. 1 and 2). Given the $m3m$ cubic point group symmetry of the underlying fluorite-type parent structure, there are at least 12 and potentially up to 24 (initially symmetry equivalent) "primary" modulation wave-vectors (14) of $\sim\frac{1}{8}\langle 224\rangle_F^*$ type. The local symmetry depends upon how many of these primary modulation wave-vectors are simultaneously excited in any one local real space region.

Note that any lowering of local symmetry could be expected to be accompanied by twinning (see, for example, the twinned $\langle 110\rangle_F$ type zone axis EDP of the α_1' phase shown in Fig. 3), particularly in the case of the α_1' phase where the rhombohedral metric distortion of the fluorite substructure is very small (5, 12, 13). It is therefore important to be sure that any EDP's come from a single domain real space region. Such multi-$\mathbf{q}$ problems are endemic in modulated structures involving relatively small amplitude distortions away from a high symmetry parent structure (see, for example, (15)). In the current case, the scale of the twinning was (fortunately) found to be sufficiently large that single domain EDPs (as shown in Figs. 1 and 2) could relatively easily be obtained.

In agreement with the XRD results of Conflant *et al.* (5) for the α_1'' phase and of Roth and colleagues (12, 13) for both the α_1' and α_1'' phases, the satellite reflections accompanying the strong fluorite type substructure Bragg reflections were found to be consistent with a lowering of the cubic $m3m$ point group symmetry of fluorite to rhombohedral $\bar{3}m$ point group symmetry in both cases. The type of rhombohedral symmetry, however, was found to be quite distinct (cf., for example, Fig. 1a with Fig. 1c and Fig. 1b with Fig. 1d.

The α_1' Phase

In the case of the α_1' phase, three sets of satellite reflections of $\mathbf{G}_F \pm \sim\frac{1}{8}\langle 224\rangle_F^*$ type were found to be strongly excited. The corresponding primary modulation wave-vectors (14) were $\mathbf{q}_1' \sim \frac{1}{8}[224]_F^*$, $\mathbf{q}_2' \sim \frac{1}{8}[422]_F^*$, and $\mathbf{q}_3' \sim \frac{1}{8}[242]_F^*$

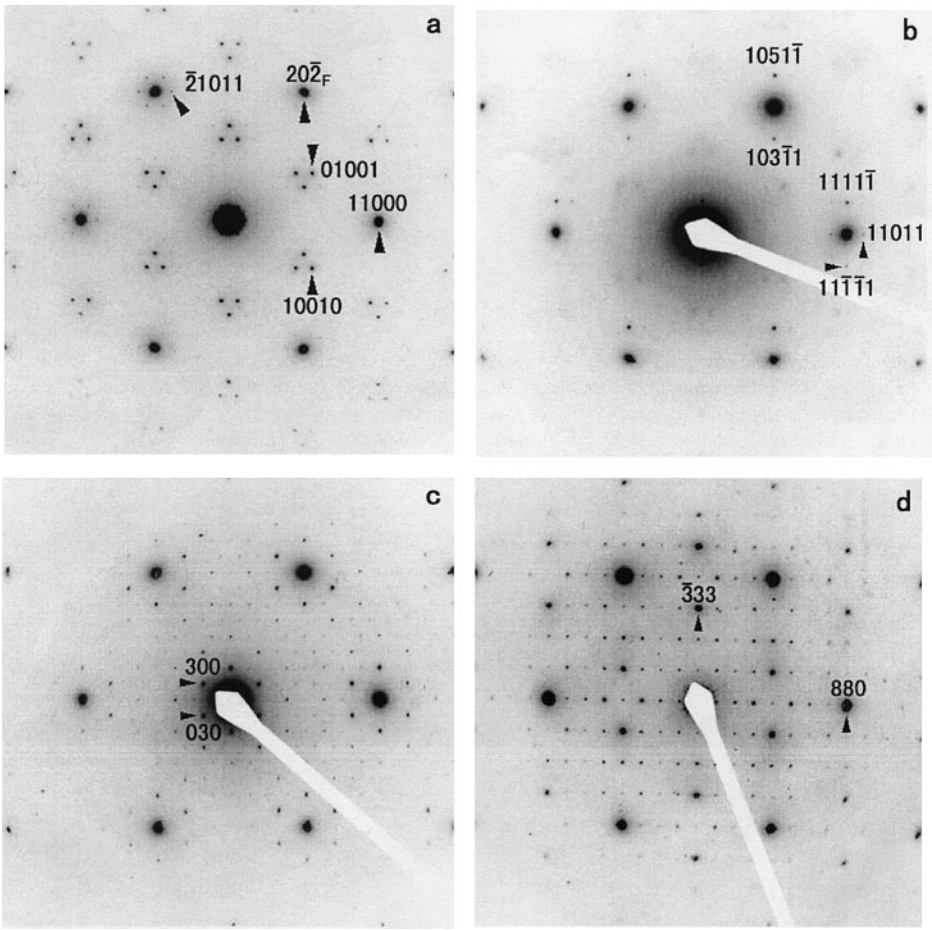

FIG. 1. The two distinct types of $\langle 111\rangle_F$ zone axis electron diffraction patterns (EDPs) characteristic of the rhombohedral (a), (b) α_1' and (c), (d) α_1'' phases. A fluorite substructure reflection, $[20\bar{2}]_F^*$, is labeled in (a). The strongest satellite reflections characteristic of both the α_1' and α_1'' phases were always found to be of $\mathbf{G}_F \pm \sim\frac{1}{8}\langle 224\rangle_F^*$ type (F for fluorite), where $\mathbf{G}_F$ represents the strong Bragg reflections of the underlying ($Fm\bar{3}m$) fluorite-type parent structure (see, for example, the reflections labeled 10010 and 01001 in (a), $1111\bar{1}$ and $1051\bar{1}$ in (b), 300 and 030 in (c), and $\bar{3}33$ in (d). Indexation in (a) and (b) is with respect to the five basis vectors $\mathbf{M}^* = \{\mathbf{a}_H^*, \mathbf{b}_H^*, \mathbf{c}_H^*, \mathbf{q}_1 = \varepsilon\mathbf{a}_H^*, \mathbf{q}_2 = \varepsilon\mathbf{b}_H^*\}$ (see the text for details). Indexation in (c) and (d) is with respect to an $R\bar{3}m$ ($\mathbf{a}_H = 8\times\frac{1}{2}[01\bar{1}]_F$, $\mathbf{b}_H = 8\times\frac{1}{2}[\bar{1}01]_F$, $\mathbf{c}_H = [111]_F$; $\mathbf{a}_H^* = \frac{1}{24}[\bar{2}4\bar{2}]_F^*$, $\mathbf{b}_H^* = \frac{1}{24}[\bar{4}22]_F$, $\mathbf{c}_H^* = \frac{1}{3}[111]_F^*$ in the hexagonal setting [subscript H] of $R\bar{3}m$) rhombohedral fluorite supercell.

respectively. Close inspection of Figs. 1a and 1b and, in particular, of Fig. 2a, however, shows that these primary modulation wave-vectors are in fact incommensurable with respect to the (necessarily) rhombohedrally distorted fluorite substructure and of the form $\mathbf{q}_1' = \frac{1}{3}[111]_F^* + \varepsilon\frac{1}{3}[\bar{2}\bar{2}4]_F^*$, $\mathbf{q}_2' = \frac{1}{3}[111]_F^* + \varepsilon\frac{1}{3}[4\bar{2}\bar{2}]_F^*$ and $\mathbf{q}_3' = \frac{1}{3}[111]_F^* + \varepsilon\frac{1}{3}[\bar{2}4\bar{2}]_F^*$, with ε weakly dependent upon composition across the α_1' solid solution field. Although no attempt has been made to measure ε systematically as a function of composition and temperature across the solid solution field, it is clear from careful Guinier and XRD work that it does indeed vary slightly as a function of composition (as first reported by Conflant *et al.* (5)) and takes a value in the vicinity of 0.11. At $x = 0.274$, for example, ε was determined to be 0.109(1)—as can be measured from Fig. 2a. Note that $\varepsilon = \frac{1}{8} = 0.125$ corresponds to the value of ε at which $\mathbf{q}_1' = \frac{1}{8}[224]_F^*$, $\mathbf{q}_2' = \frac{1}{8}[422]_F^*$ and $\mathbf{q}_3' = \frac{1}{8}[242]_F^*$ exactly (cf. Fig. 2a with Fig. 2b). The clear incommensurability of these primary modulation wave-vectors in the case of the α_1' phase explains the weak composition dependence of the satellite reflections first reported by Conflant *et al.* (5).

Such a set of incommensurate primary modulation wave-vectors is strongly reminiscent of the so-called $1T_1$ and $1T_2$ polymorphs of TaS_2 (16), both of which are characterized by a set of incommensurate primary modulation wave-vectors related by three-fold symmetry and which can be broken into a commensurable wave-vector component along the threefold direction and an incommensurable component along the orthogonal basal plane directions of reciprocal space. Note that $\mathbf{q}_1' + \mathbf{q}_2' + \mathbf{q}_3' = [111]_F^*$ exactly regardless of the value of ε. There is therefore a corresponding Landau free energy term which "locks in" the component of the

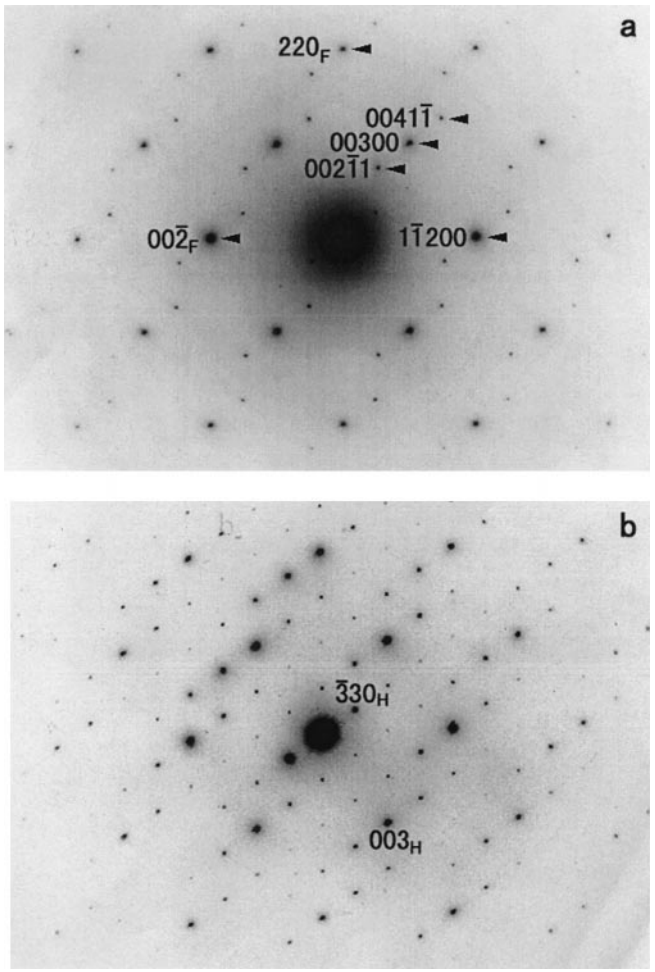

FIG. 2. $\langle 110\rangle_F$ zone axis electron diffraction patterns (EDPs) characteristic of the rhombohedral (a) α_1' and (b) α_1'' phases. The reflection $[220]_F^*$ is labeled in (a). The strongest satellite reflections characteristic of both the α_1' and (b) α_1'' phases were again found to be of $\mathbf{G}_F \pm \sim \frac{1}{8}\langle 224\rangle_F^*$ type (see, for example, the reflections labeled $0041\bar{1}$ and $002\bar{1}1$ in (a) and $\bar{3}30$ in (b). Indexation in (a) is with respect to the five basis vectors $\mathbf{M}^* = \{\mathbf{a}_H^*, \mathbf{b}_H^*, \mathbf{c}_H^*, \mathbf{q}_1 = \varepsilon\mathbf{a}_H^*, \mathbf{q}_2 = \varepsilon\mathbf{b}_H^*\}$ while indexation in (b) is with respect to $\mathbf{a}_H^* = \frac{1}{24}[\bar{2}42]_F^*$, $\mathbf{b}_H^* = \frac{1}{24}[\bar{4}22]_F$, $\mathbf{c}_H^* = \frac{1}{3}[111]_F^*$.

primary modulation wave-vector along the $[111]_F^*$ reciprocal space direction without locking in the orthogonal $\varepsilon\frac{1}{3}\langle\bar{2}\bar{2}4\rangle_F^*$ components (17).

Given the rhombohedral symmetry of the primary modulation wave-vectors, it is clear that the space group symmetry of the average fluorite substructure must necessarily be lowered to $R\bar{3}m$ ($\mathbf{a}_H = \frac{1}{2}[0\bar{1}1]_F$, $\mathbf{b}_H = \frac{1}{2}[10\bar{1}]_F$, $\mathbf{c}_H = [111]_F$; $\mathbf{a}_H^* = \frac{1}{3}[2\bar{4}2]_F^*$, $\mathbf{b}_H^* = \frac{1}{3}[4\bar{2}\bar{2}]_F$, $\mathbf{c}_H^* = \frac{1}{3}[111]_F^*$ in the hexagonal setting [subscript H] of $R\bar{3}m$ with a fully occupied average metal ion at $(000)_H$ and a partially occupied oxygen ion at $(00z)_H$, $z \sim \frac{1}{4}$). Note that the primary modulation wave-vectors $\mathbf{q}_1' = \mathbf{c}_H^* + \varepsilon(\mathbf{a}_H^* - \mathbf{b}_H^*)$, $\mathbf{q}_2' = c_H^* + \varepsilon\mathbf{b}_H^*$ and $\mathbf{q}_3' = c_H^* - \varepsilon\mathbf{a}_H^*$ with respect to this rhombohedral sub-cell. Reciprocal space can then be indexed in terms of integer ($hklmn$) combinations of the 5 basis vectors $\{\mathbf{a}_H^*, \mathbf{b}_H^*, \mathbf{c}_H^*, -\mathbf{q}_3' = -\mathbf{c}_H^* + \varepsilon a_H^*, \mathbf{q}_2' = \mathbf{c}_H^* + \varepsilon\mathbf{b}_H^*\}$. (Because $\mathbf{q}_1' + \mathbf{q}_2' + \mathbf{q}_3' = [111]_F^* = [003]_H^*$, there are really only two linearly independent primary modulation wave vectors). Alternatively the rational $\mathbf{c}_H^*$ component of the two incommensurate primary modulation wave vectors) can be incorporated into the third integer index so that reciprocal space is indexed with respect to the five basis vectors $\mathbf{M}^* = \{\mathbf{a}_H^*, \mathbf{b}_H^*, \mathbf{c}_H^*, \mathbf{q}_1 = \varepsilon\mathbf{a}_H^*, \mathbf{q}_2 = \varepsilon\mathbf{b}_H^*\}$ as has been done in Figs. 1a and 1b and 2a.

The observed reciprocal space Bravais lattice centering condition (18) is then given by $F(HKLMN) = 0$ unless $-H+K+L+M-N = 3n$ (H, K, L, M, N, n all integers) corresponding to the superspace centering operation $\{x_1 - \frac{1}{3}, x_2 + \frac{1}{3}, x_3 + \frac{1}{3}, x_4 + \frac{1}{3}, x_5 - \frac{1}{3}\}$. The absence of any other systematic absence condition in conjunction with the $\bar{3}m$ Laue symmetry suggests a (3 + 2)-dimensional superspace group symmetry of $R\bar{3}m(\varepsilon 00)11$ with superspace generating operations given by $\{x_1 - \frac{1}{3},\ x_2 + \frac{1}{3},\ x_3 + \frac{1}{3}, x_4 + \frac{1}{3}, x_5 - \frac{1}{3}\}$, $\{-x_1, -x_2, -x_3, -x_4 + 2\delta_1, -x_5 + 2\delta_2\}$, $\{-x_2,\ x_1 - x_2,\ x_3,\ -x_5 + \delta_1 + \delta_2,\ x_4 - x_5 - \delta_1 + 2\delta_2\}$ and $\{-x_2, -x_1, x_3,\ -x_5 + \delta_1 + \delta_2,\ -x_4 + \delta_1 + \delta_2\}$ respectively. With the help of these superspace generating operations it is then possible to generate the symmetry-constrained forms of the compositional and displacive atomic modulation functions (AMFs) describing the deviation of the modulated structure from its underlying $R\bar{3}m$ fluorite-type average structure (see below).

Note that the intensity of the observed incommensurate satellite reflections clearly drops off very rapidly with increasing harmonic order, e.g., only a very few, rather weak satellite reflections of second or higher order are apparent in EDPs (see, for example, the reflection labeled $[\bar{2}1011]^*$ in Fig. 2a and that labeled $[11011]^*$ in Fig. 1b). Given that EDPs, as a result of dynamical diffraction, always tends to show more higher order harmonic satellite reflections than can be measured via (kinematical) X-ray diffraction, it must therefore be a not unreasonable approximation to put all compositional and displacive modulation wave amplitudes of higher order than first to zero in such AMFs.

The fact that the atomic scattering factor difference between Bi and Ca for X-rays, $f_{Bi} - f_{Ca}$, *is* ~ 7.9 times the atomic scattering factor difference between an oxygen ion and a vacancy, i.e., f_0, (at $\theta = 0°$) ensures that Ca/Bi metal ion ordering and associated structural relaxation makes the dominant contribution to the incommensurate satellite reflections in XRD profiles. The clear presence of the low angle ($2\theta \sim 9.8°$) $[0011\bar{1}]^*$ satellite reflection in XRD profiles (see Fig. 6 and Table 7 of (13)), where compositional ordering is highly likely to make the major contribution to the structure factor of the relevant satellite reflection, provides clear evidence for Ca/Bi ordering on the (slightly rhombohedrally distorted) essentially ccp cation array (see Fig. 4).

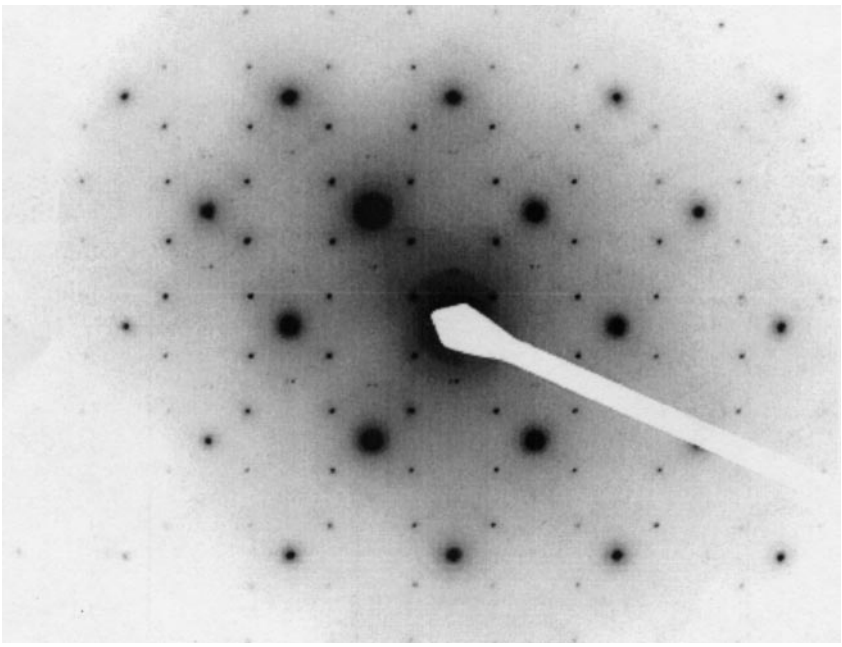

FIG. 3. Shows a twinned $\langle 110\rangle_F$ type zone axis EDP of the α_1' phase (cf. Fig. 2a).

The α_1'' Phase

In the case of the α_1'' phase, three sets of satellite reflections of $\mathbf{G}_F \pm \sim\frac{1}{8}\langle 224\rangle_F^*$ type were again found to be strongly excited. The corresponding primary modulation wave-vectors this time, however, were found to be orthogonal to the unique threefold axis, exactly commensurate and given by $\mathbf{q}_1 = \frac{1}{8}[\bar{2}\bar{2}4]_F^*$, $\mathbf{q}_2 = \frac{1}{8}[4\bar{2}\bar{2}]_F^*$ and $\mathbf{q}_3 = \frac{1}{8}[\bar{2}4\bar{2}]_F^*$ (see the reflections labeled $[\bar{3}30]$*, $[0\bar{3}0]$*, and $[300]$* in Figs. 1c and 2b); i.e., the α_1'' phase is a genuine commensurately modulated, or superstructure, phase. While satellite reflections of the form $\mathbf{G}_F \pm \mathbf{q}_1$, $\mathbf{G}_F \pm \mathbf{q}_2$, and $\mathbf{G}_F \pm \mathbf{q}_3$ were always much stronger than all other satellite reflections (see Figs. 1c, 1d, and 2b), it was nonetheless clear that many more higher order harmonic satellite reflections were visible than was the case for the α_1' phase (cf. Figs. 1c and 1d with Figs. 1a and 1b and Figs. 2b with 2a).

As for the α_1' phase, the rhombohedral symmetry of the (commensurate) primary modulation wave-vectors necessarily lowers the resultant space group symmetry to $R\bar{3}m$ ($\mathbf{a}_H = 8\times\frac{1}{2}[01\bar{1}]_F$, $\mathbf{b}_H = \mathbf{8}\times\frac{1}{2}[\bar{1}01]_F$, $\mathbf{c}_H = [111]_F$; $\mathbf{a}_H^* = \frac{1}{24}[\bar{2}4\bar{2}]_F^*$, $\mathbf{b}_H^* = \frac{1}{24}[\bar{4}22]_F$, $\mathbf{c}_H^* = \frac{1}{3}[111]_F^*$ in the hexagonal setting [subscript H] of $R\bar{3}m$). Indexation in Figs. 1c, 1d, and 2b is with respect to this rhombohedral fluorite supercell. This rhombohedral cell is consistent with the second of the cells suggest for this phase by Burton *et al.* (13), i.e., $R\bar{3}$, $a = 30.4640(5)$, $c = 9.6477$ Å. (The alternative $B2/m$, $a = 15.5819(3)$, $b = 3.8077(1)$, $c = 10.8955(3)$ Å, $\beta = 91.829(2)^\circ$ monoclinic cell suggested by Burton *et al.* (13) corresponds to the choice $\mathbf{a} = [2\bar{2}0]_F$, $\mathbf{b} = \frac{1}{2}[110]_F$, $\mathbf{c} = [002]_F$; $\mathbf{a}^* = \frac{1}{8}[2\bar{2}0]_F^*$, $\mathbf{b}^* = \frac{1}{2}[220]_F^*$, $\mathbf{c}^* = \frac{1}{4}[002]_F^*$ with $[101]^* = \frac{1}{8}[2\bar{2}4]_F^*$ and $[10\bar{1}]^* = \frac{1}{8}[2\bar{2}\bar{4}]_F^*$ but is incompatible with the observed electron diffraction evidence).

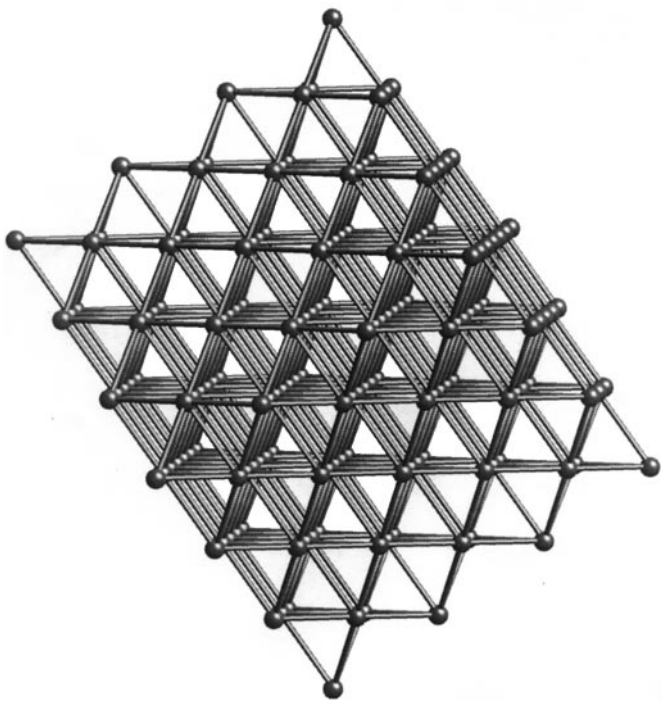

FIG. 4. Ca/Bi ordering on this (slightly rhombohedrally distorted) essentially ccp cation array is primarily responsible for the observed satellite reflections of the α_1' phase. The projection axis shown is close to $[110]_H$ with $\mathbf{c}_H$ vertical.

While there is nothing incorrect about describing the α_1'' phase as a conventional superstructure phase, the hierarchical intensity distribution of the observed satellite reflections (with low order modulation harmonics strongest in intensity and apparently diminishing more or less systematically in intensity as the harmonic order increases) suggests the value of a modulated structure, rather than conventional superstructure, approach to structural characterization (19). It is therefore useful to describe the α_1'' phase using the same formalism as given above for the α_1' phase, i.e., in terms of a (commensurately modulated), slightly rhombohedrally distorted fluorite substructure.

This latter substructure ($R\bar{3}m$: $\mathbf{a}_H = \frac{1}{2}[0\bar{1}1]_F$, $\mathbf{b}_H = \frac{1}{2}[10\bar{1}]_F$, $\mathbf{c}_H = [111]_F$; $\mathbf{a}_H^* = \frac{1}{3}[2\bar{4}2]_F^*$, $\mathbf{b}_H^* = \frac{1}{24}[4\bar{2}\bar{2}]_F$, $\mathbf{c}_H^* = \frac{1}{3}[111]_F^*$) is in essence the same as for the α_1' phase. The (primitive) primary modulation wave vectors (with respect to this rhombohedral subcell) for the α_1'' phase are given by $\mathbf{q}_1 = \varepsilon\mathbf{a}_H^*$ and $\mathbf{q}_2 = \varepsilon\mathbf{b}_H^*$, with $\varepsilon = \frac{3}{8}$. This time there is no longer a rational $\mathbf{c}_H^*$ component (cf. with the (primitive) primary modulation wave-vectors for the α_1' phase of $-\mathbf{c}_H^* + \varepsilon\mathbf{a}_H^*$ and $\mathbf{c}_H^* + \varepsilon\mathbf{b}_H^*$ respectively). In addition, $\varepsilon = \frac{3}{8}$ is commensurate and ~ 3 times larger than the ~ 0.11 value characteristic of the α_1' phase.

4. REAL SPACE INTERPRETATION

While it is beyond the scope of the current paper to attempt to determine the structures of these rather complex (α_1' and α_1'') phases, it is possible to derive an expression for the Ca/Bi metal ion ordering largely responsible for the observed satellite reflections using a modulation wave approach to structural characterization. We focus largely in what follows on Ca/Bi metal ion ordering both because there is strong experimental evidence that it plays a dominant role and also because the satellite reflections exist at elevated temperatures where the oxygen ions are essentially mobile (5).

Underlying Fluorite-Related Average Structure

The underlying average structure of the $(1-x)\frac{1}{2}Bi_2O_3\cdot xCaO$, $0.20 < x < 0.29$, α_1' (and α_1'') phase can safely be assumed to be of (slightly rhombohedrally distorted) fluorite-type, space group symmetry $R\bar{3}m$ ($\mathbf{a}_H = \frac{1}{2}[0\bar{1}1]_F$, $\mathbf{b}_H = \frac{1}{2}[10\bar{1}]_F$, $\mathbf{c}_H = [111]_F$). There are then three average ions per primitive unit cell: a fully occupied metal ion M at $\mathbf{r}_M = 000$ (average atomic scattering factor $f_M^{av} = (1-x)f_{Bi} + xf_{Ca}$) and two partially occupied oxygen ions, O1 at $\mathbf{r}_{O1} = 00z$ ($z \sim \frac{1}{4}$) and the inversion symmetry related O2 at $\mathbf{r}_{O2} = 00\bar{z}$ respectively (average scattering factors $f_O^{av} = \frac{1}{4}(3-x)f_O$).

Atomic Modulation Functions (AMFs)

The three-dimensional compositional and displacive AMFs describing the perturbations away from these average occupancies and positions depend upon $(\mathbf{r}_\mu + \mathbf{T})$, i.e., the position of the μth ion ($\mu = M$, O1 or O2) in the $\mathbf{T}$th ($\mathbf{T} = u\mathbf{a}_F + v\mathbf{b}_F + w\mathbf{c}_F$; u, v, w integers) unit cell of the average structure (14, 20), and can be written in the form:

$$\delta f_\mu(\mathbf{r}_\mu+\mathbf{T}) = f_\mu^{av}\Sigma_{MN}a_\mu(MN)\cos\{2\pi(M\mathbf{q}_1+N\mathbf{q}_2)\cdot(\mathbf{r}_\mu+\mathbf{T}) + \theta_\mu(MN)\}, \quad [1]$$

and

$$\mathbf{u}_\mu(\mathbf{r}_\mu+\mathbf{T}) = \Sigma_{\alpha=a,b,c}\Sigma_{MN}\boldsymbol{\alpha}\varepsilon_{\mu\alpha}(MN)\cos\{2\pi(M\mathbf{q}_1+N\mathbf{q}_2)\cdot(\mathbf{r}_\mu+\mathbf{T}) + \theta_{\mu\alpha}(MN)\}, \quad [2]$$

respectively, where M and N are integers and label the particular modulation wave harmonic. Note that $a_\mu(\bar{M}\bar{N}) = a_\mu(MN)$, $\theta_\mu(\bar{M}\bar{N}) = -\theta_\mu(MN)$, $\varepsilon_{\mu\alpha}(\bar{M}\bar{N}) = \varepsilon_{\mu\alpha}(MN)$, $\theta_{\mu\alpha}(\bar{M}\bar{N}) = -\theta_{\mu\alpha}(MN)$, etc. Determination of the above modulation wave amplitudes and phases essentially constitutes structure refinement.

In the language of superspace (18, 20), the desired resultant fractional coordinates in three-dimensional physical space, i.e., the x, y, z components of $(\mathbf{r}_\mu + \mathbf{T} + \mathbf{u}_\mu(\mathbf{r}_\mu + \mathbf{T}))$, are labeled x_1, x_2, and x_3 respectively. The corresponding perpendicular space fractional co-ordinates are given by $x_4 = \mathbf{q}_1\cdot(\mathbf{r}_\mu + \mathbf{T} + \mathbf{u}_\mu(\mathbf{r}_\mu + \mathbf{T}))$ and $x_5 = \mathbf{q}_2\cdot(\mathbf{r}_\mu + \mathbf{T} + \mathbf{u}_\mu(\mathbf{r}_\mu + \mathbf{T}))$ respectively. Superspace symmetry is expressed in terms of the effect of the particular symmetry operation upon the fractional coordinates $\{x_1, \ldots, x_5\}$ (18, 20).

The $R\bar{3}m(\varepsilon 00)11$ superspace group symmetry of the α_1' phase can now be used to constrain the form of the compositional and/or displacive AMF's given above, i.e., to minimize the number of independent structural variables that need to be determined in any subsequent structure refinement. In the case of the metal ion compositional AMF, for example, systematic application of the superspace generating operations given above leads to the following expression:

$$\begin{aligned}\delta f_M(\mathbf{T})/f_M^{av} = a_M\{&\cos(2\pi[-(-\mathbf{c}_H^* + \varepsilon\mathbf{a}_H^*)\cdot\mathbf{T} + \delta_1]) \\ &+ \cos(2\pi[(\mathbf{c}_H^* + \varepsilon\mathbf{b}_H^*)\cdot\mathbf{T} - \delta_2]) \\ &+ \cos(2\pi[(\mathbf{c}_H^* + \varepsilon\mathbf{a}_H^* - \varepsilon\mathbf{b}_H^*)\cdot\mathbf{T} - \delta_1 + \delta_2])\} \\ &+ \cdots \text{Higher order harmonic terms} \cdots. \end{aligned} \quad [3]$$

The fact that the only clearly observed satellite reflections in the case of the α_1' phase (see Figs. 1 and 2) are of the form $\mathbf{G}_F \pm \mathbf{q}_i'$ ($\mathbf{q}_1' = \mathbf{c}_H^* + \varepsilon(\mathbf{a}_H^* - \mathbf{b}_H^*)$, $\mathbf{q}_2' = \mathbf{c}_H^* + \varepsilon\mathbf{b}_H^*$ and $\mathbf{q}_3' = \mathbf{c}_H^* - \varepsilon\mathbf{a}_H^*$) requires that the corresponding compositional and displacive modulation wave amplitudes are the major (if not the only) nonzero amplitudes. Hence only these first order terms are given explicitly in the above expression.

Use of these primitive primary modulation wave-vectors in Eq. [3] ensures that **T** above need not be limited to $u\mathbf{a}_F + v\mathbf{b}_F + w\mathbf{c}_F$ (u, v, w integers) but rather can be taken as representing all average structure Bravais lattice vectors including $\pm\frac{1}{3}(\mathbf{a} + \mathbf{b} + \mathbf{c})$ etc. Note that the compositional AMF of Eq. [3] is a direct function of $\bar{x}_4 - \delta_1 = \mathbf{q}_1 \cdot \mathbf{T} - \delta_1 = \varepsilon \mathbf{a}_H^* \cdot \mathbf{T} - \delta_1 \equiv t_1 - \delta_1$ and $\bar{x}_5 - \delta_2 = \mathbf{q}_2 \cdot \mathbf{T} - \delta_2 = \varepsilon \mathbf{b}_H^* \cdot \mathbf{T} - \delta_2 \equiv t_2 - \delta_2$ respectively.

Because ε is incommensurable with respect to the underlying substructure, $\delta f_M(\mathbf{T})$ is not a period function of T and hence it is not possible to draw a particular Ca/Bi ordering pattern resulting from Eq. [3]. (A further consequence is that all possible values of $(t_1 - \delta_1)$ and $(t_2 - \delta_2)$ will occur at some point, **T**, in the structure. Hence AMFs are ideally determined as a function of $(t_1 - \delta_1)$ and $(t_2 - \delta_2)$—see below). It is, however, possible to draw some general conclusions about Ca/Bi ordering from Eq. [3]. For example, because ε is small (~ 0.109 in the case of the α_1' phase), it is clear that Bi and Ca ions must separately cluster together in fairly largish clusters within each close packed metal atom layer perpendicular to $\mathbf{c}_H$, i.e., a phase change of 180° in any one of the modulation waves in Eq. [3] requires a considerable real space shift of $\Delta\mathbf{T} \sim 4$–$5\mathbf{a}_H$ or $\mathbf{b}_H$. In the case of the α_1'' phase, by contrast, where $\varepsilon = \frac{3}{8}$ is rather larger, the size of any such clusters of like type will be much reduced.

Furthermore, the $\mathbf{c}_H^*$ component of each of the modulation wave-vectors in Eq. [3] implies a phase shift of 120° in each of the modulation waves from one close packed metal atom layer to the next (see Fig. 4) and ensures a rhombohedral stacking of Ca-rich and Bi-rich regions from one close packed metal atom layer to the next. In the case of the α_1'' phase by contrast (see Fig. 1c), the corresponding primitive primary modulation wave-vectors do not have a $\mathbf{c}_H^*$ component so that any Ca-rich and Bi-rich regions in a close packed metal atom layer will stack on top of one another along the $\mathbf{c}_H$ real space direction.

Finally, having parameterized the metal ion compositional AMF, it remains to consider its two-dimensional shape in hyperspace (i.e., as functions of $(t_1 - \delta_1)$ and $(t_2 - \delta_2)$). This is shown in Fig. 5. (Two hyperspace unit cells are shown along each of the $(t_1 - \delta_1)$ and $(t_2 - \delta_2)$ axes). Note that contours parallel to each other in hyperspace, on each of which the metal ion composition is constant are defined by equations of the form

$$\cos(-2\pi[t_1 - \delta_1]) + \cos(2\pi[t_2 - \delta_2]) + \cos(2\pi[(t_1 - \delta_1) - (t_2 - \delta_2)]) = \text{constant}. \quad [4]$$

Such contours can also be considered to divide hyperspace up into congruent areas—one Bi-rich and the other Ca-rich with respect to the average metal ion composition.

By choosing the value of the constant in Eq. [4] and hence the dividing contour appropriately, it is possible to divide hyperspace such that the ratio of the area of hyperspace on the side of the contour to the other matchs any particular desired Bi/Ca ratio. The heavy lines in Fig. 5, for example, show the contour that results if the constant in Eq. [4] is put equal to -1.0. (Note that the value of the function in the centre of the hexagonal region is $+3.0$ while that in the center of the triangular regions is -1.5). In this case, the ratio of the hexagonal areas of hyperspace on the side of this contour to the triangular areas on the other side is 3:1 corresponding to the Bi/Ca ratio for $x = 0.25$ in the middle of the α_1' solid solution field. A Bi or a Ca ion can then be ascribed to any particular value of **T** dependent upon the corresponding values of $(t_1 - \delta_1)$ and $(t_2 - \delta_2)$ and its positioning with respect to the relevant contour. Adjusting x across the solid solution corresponds to adjusting the value of the constant in Eq. [4] above around the value -1.0.

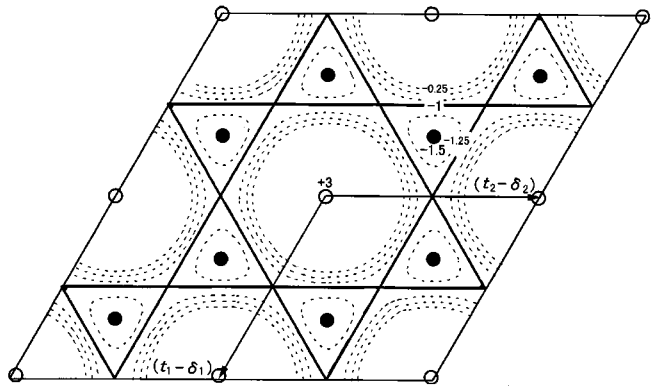

FIG. 5. Shows the two-dimensional "shape" of the metal ion compositional AMF in hyperspace (i.e., as functions of $(t_1 - \delta_1)$ and $(t_2 - \delta_2)$). Contours parallel to each other in hyperspace, on each of which the metal ion composition is constant, are shown.

Further consideration, however, is beyond the scope of the current contribution.

ACKNOWLEDGMENT

Dr. Y. Tabira is gratefully acknowledged for considerable help with production of the figures.

REFERENCES

1. T. Takahashi and H. Iwahara, *Mater. Res. Bull.* **13,** 1447 (1978).
2. A. W. Sleight, *Science* **208,** 895–900 (1980).
3. L. G. Sillen and B. Aurivillius, *Z. Kristallogr.* **101,** 483 (1939).
4. E. M. Levin and R. S. Roth, *J. Res. Nat. Bur. Stand. A* **68,** 197 (1964).
5. P. Conflant, J-C. Boivin, and D. Thomas, *J. Solid State Chem.* **18,** 133 (1976).
6. R. Guillermo, P. Conflant, J-C. Boivin, and D. Thomas, *Rev. Chim. Miner.* **15,** 153 (1978).

7. T. Takahashi, H. Iwahara, and T. Arao, *J. Appl. Electrochem.* **5,** 187 (1975).
8. M. J. Verkerk, K. Keizer, and A. J. Burggraaf, *J. Appl. Electrochem.* **10,** 81 (1980).
9. C. D. Ling, R. L. Withers, S. Schmid, and J. G. Thompson, *J. Solid State Chem.* **137,** 42 (1998).
10. T. Takahashi, H. Iwahara, and Y. Nagai, *J. Appl. Electrochem.* **2,** 97 (1972).
11. M. J. Verkerk, G. M. H. van de Velde, A. J. Burggraaf, and R. B. Helmholdt, *J. Phys. Chem. Solids* **43,** 1129 (1982).
12. R. S. Roth, N. M. Hwang, C. J. Rawn, B. P. Burton, and J. J. Ritter, *J. Am. Ceram. Soc.* **74,** 2148 (1991).
13. B. P. Burton, C. J. Rawn, R. S. Roth, and N. M. Hwang, *J. Res. NIST* **98,** 469 (1993).
14. J. M. Pérez-Mato, G. Madariaga, and M. J. Tello, *J. Phys. C* **19,** 2613 (1986).
15. D. J. Eaglesham, R. L. Withers, and D. M. Bird, *J. Phys. C* **19,** 359 (1986).
16. R. L. Withers and J. W. Steeds, *J. Phys. C* **20,** 4019 (1987).
17. M. B. Walker and R. L. Withers, *Phys. Rev. B* **28,** 2766 (1983).
18. S. van Smaalen, *Cryst. Rev.* **4,** 79 (1995).
19. J. M. Pérez-Mato. *in* "Methods of Structural Analysis of Modulated Structures and Quasi-Crystals," (J. M. Pérez-Mato, F. J. Zuniga and G. Madariaga, Eds.), pp. 117–128. World Scientific, Singapore, 1991.
20. R. L. Withers, S. Schmid, and J. G. Thompson, *Prog. Solid State Chem.* **26,** 1 (1998).